Journal of
MATERIALS RESEARCH

Influences of pileup on the measurement of mechanical properties by load and depth sensing indentation techniques

A. Bolshakov[a] and G. M. Pharr
Department of Materials Science, Rice University, 6100 Main Street, Houston, Texas 77005-1892

(Received 8 May 1997; accepted 16 October 1997)

Finite element simulation of conical indentation of a wide variety of elastic-plastic materials has been used to investigate the influences of pileup on the accuracy with which hardness and elastic modulus can be measured by load and depth-sensing indentation techniques. The key parameter in the investigation is the contact area, which can be determined from the finite element results either by applying standard analysis procedures to the simulated indentation load-displacement data, as would be done in an experiment, or more directly, by examination of the contact profiles in the finite element mesh. Depending on the pileup behavior of the material, these two areas may be very different. When pileup is large, the areas deduced from analyses of the load-displacement curves underestimate the true contact areas by as much as 60%. This, in turn, leads to overestimations of the hardness and elastic modulus. The conditions under which the errors are significant are identified, and it is shown how parameters measured from the indentation load-displacement data can be used to identify when pileup is an important factor.

I. INTRODUCTION

Numerous methods have been developed in recent years for measuring the mechanical properties of materials by means of load and depth sensing indentation testing.[1–3] One of the great advantages of these methods is that it is not necessary to measure the area of the hardness impression by imaging; rather, the contact area and the material properties which can be derived from it are determined from analyses of indentation load-displacement data. The methods form the basis for nanoindentation testing, in which mechanical properties can be measured from very small indentations, sometimes only a few nanometers deep.[4,5] Among the properties that can be measured in this way are the hardness, H, and the elastic modulus, E.

One of the more commonly used methods for analyzing nanoindentation load-displacement data is that of Oliver and Pharr,[3] which expands on ideas developed by Loubet *et al.*[1] and Doerner and Nix,[2] but is not constrained by the assumption of a flat punch indenter geometry. In the Oliver–Pharr method, hardness and elastic modulus are determined from indentation data obtained during one complete cycle of loading and unloading. The analysis begins by fitting the unloading curve to the power-law relation

$$P = B(h - h_f)^m, \tag{1}$$

where P is the indentation load, h is the displacement, B and m are empirically determined fitting parameters, and h_f is the final displacement after complete unloading (also determined by curve fitting). The unloading stiffness, S, that is, the slope of the unloading curve during the initial stages of unloading, is then established by differentiating Eq. (1) at the maximum depth of penetration, $h = h_{\max}$, giving

$$S = \frac{dP}{dh}(h = h_{\max}) = mB(h_{\max} - h_f)^{m-1}. \tag{2}$$

The depth along which contact is made between the indenter and the specimen, h_c, can also be estimated from the load-displacement data using:

$$h_c = h_{\max} - \epsilon \frac{P_{\max}}{S}, \tag{3}$$

where $P_{\max}$ is the peak indentation load and ϵ is a constant which depends on the geometry of the indenter. With these basic measurements, the projected contact area of the hardness impression, A, is derived by evaluating an empirically determined indenter shape function at the contact depth, h_c; that is, $A = f(h_c)$. The shape function $A = f(d)$ relates the cross-sectional area of the indenter to the distance back from its tip, d. Finally, the hardness, H, and effective elastic modulus, E_{eff}, are derived from

$$H = \frac{P_{\max}}{A} \tag{4}$$

[a]Current address: Baker Hughes Inteq, P.O. Box 670968, Houston, Texas 77267-0968.

 © 1998 Materials Research Society

and

$$E_{\text{eff}} = \frac{\sqrt{\pi}}{2}\frac{S}{\sqrt{A}} . \tag{5}$$

An effective modulus is used in the analysis to account for the fact that elastic deformation occurs in both the specimen and the indenter. The effective modulus is related to the specimen modulus through

$$\frac{1}{E_{\text{eff}}} = \frac{1 - \nu^2}{E} + \frac{1 - \nu_i^2}{E_i} , \tag{6}$$

where E and ν are Young's modulus and Poisson's ratio for the specimen, and E_i and ν_i are the same quantities for the indenter.[3]

The attractiveness of this approach is that direct observation and measurement of the contact area is not needed for the evaluation of H and E, thus facilitating property measurement from very small indentations. Clearly, however, the accuracy with which H and E can be measured depends on how well Eqs. (2)–(5) describe the indentation deformation behavior. In this context, it is important to note these equations were derived from a purely elastic contact solution derived by Sneddon,[6] and how well they work for elastic/plastic indentation is not entirely clear. One important way in which the elastic solution fails to properly describe elastic/plastic behavior concerns the pileup or sink-in of material around the indenter. In the purely elastic contact solution, material always sinks in, while for elastic/plastic contact, material may either sink in or pile up. Since this has important effects on the indentation contact area, it is not entirely surprising that the Oliver–Pharr method has been found to work well for hard ceramics, in which sink-in predominates,[3] but significant errors can be encountered when the method is applied to soft metals that exhibit extensive pileup (see, for example, Refs. 7 and 8).

In this study, the finite element method has been used to investigate the influences of pileup on the accuracy with which hardness and elastic modulus can be measured by load and depth sensing indentation techniques. The finite element method has been employed in many previous studies to provide important insight into material behavior during elastic/plastic indentation.[8–18] The key parameter in this investigation is the projected contact area of the indentation, A, which can be determined from the finite element results either by applying the Oliver–Pharr analysis procedure to the simulated indentation load-displacement data, or more directly, by examination of the contact profiles in the finite element mesh. Depending on the pileup behavior of the material, these two areas may be very different. It will be shown that when pileup is significant, the areas deduced from the Oliver–Pharr analysis can underestimate the true contact area by as much as 60%, which through Eqs. (4) and (5) leads to important errors in the hardness and modulus. The conditions under which the errors are significant are identified, and it is shown how important clues about the significance of pileup on measurement accuracy can be obtained from parameters measurable from the indentation load-displacement data.

II. SIMULATION AND ANALYSIS PROCEDURES

Elastic/plastic indentation was simulated using the axisymmetric capabilities of the ABAQUS finite element code. The indenter was modeled as a rigid cone with a semi-vertical angle $\phi = 70.3°$, which gives the same area-to-depth ratio as the Berkovich three-sided pyramid used frequently in nanoindentation experiments and the Vickers four-sided pyramid used in microhardness testing. All simulations were performed to a depth of 500 nm using the finite element mesh and boundary conditions illustrated in Figs. 1(a) and 1(b), in which a cylindrical coordinate system is used with radial coordinate, r, and axial coordinate, z. The specimen was modeled as a cylinder 100,000 nm high and 100,000 nm in radius represented by 2806 four-node axisymmetric elements. These specimen dimensions were found to be large enough to approximate the behavior of a semi-infinite half-space, as evidenced by an insensitivity of results to further increases in specimen size. As shown in Fig. 1(a), roller boundary conditions were applied along the centerline and bottom, a free surface was modeled at the outside of the cylinder, and the interface between the indenter and the specimen was assumed to be frictionless. Figure 1(b) is included to show the region of contact, where very fine elements were used to achieve the precision needed in the measurement of contact radii and contact areas. Away from the contact, a progressively coarser mesh was employed both at the surface and in the interior of the specimen.

The constitutive behavior of the material used for the finite element modeling is shown schematically in Fig. 2, in which σ is the uniaxial stress and ϵ is the uniaxial strain. Young's modulus $E = 70$ GPa was used in all simulations, but results were generalized by appropriate nondimensionalizations to account for materials with other elastic moduli. While the majority of the simulations were conducted using Poisson's ratio $\nu = 0.25$, a limited number of simulations were performed using $\nu = 0.00$ and $\nu = 0.45$ to examine the sensitivity of results to Poisson ratio effects. Linear elasticity was assumed at all strains, and no pressure sensitivity was included in the constitutive modeling. Giannakopoulas and Larsson have recently performed three-dimensional finite element simulations of Vickers and Berkovich indentation which provide valuable insight into the effects of pressure sensitivity on indentation behavior.[18]

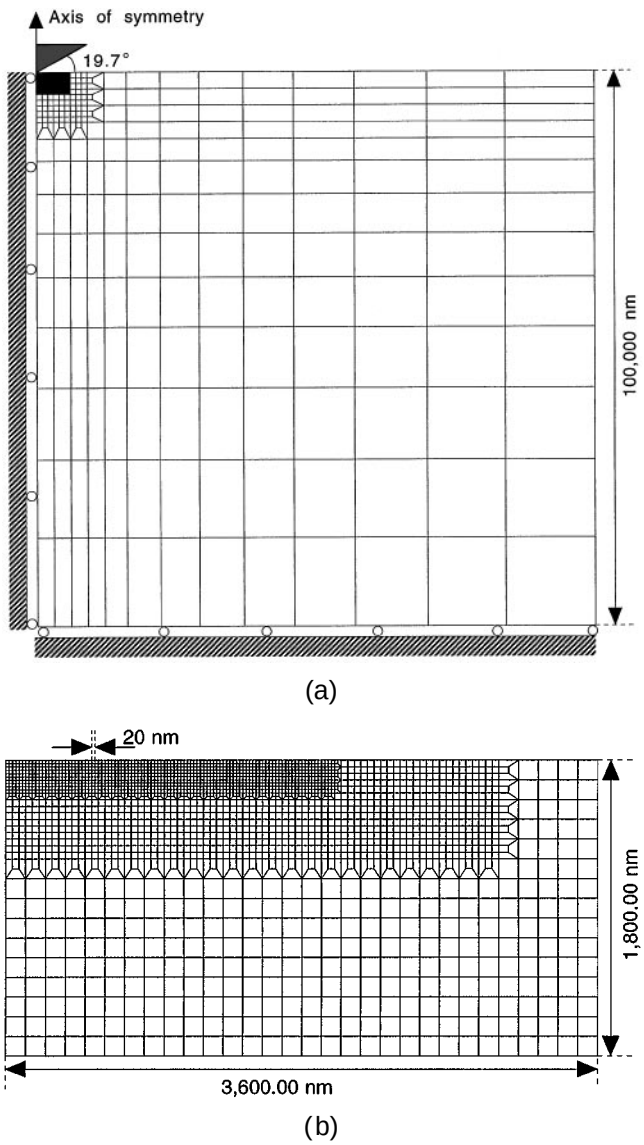

FIG. 1. The finite element mesh and boundary conditions: (a) the entire mesh; (b) details of the mesh in the region of contact.

Plasticity was modeled by assuming the material behaves as a von Mises solid with discrete yielding followed by linear, isotropic work hardening. The large strain capabilities of ABAQUS were used to account for finite strains and rotations. Yield stresses, σ_y, were varied systematically from a 0.114 GPa to 5.324 GPa. The upper limit on the yield stress was chosen to keep the elastic strains small with respect to the plastic strains, as required by the underlying elastic-plastic deformation theory. Since the elastic strains are of the order of σ_y/E, the upper limit on the yield stress places a limit on the elastic strains of about 7%. Finite element simulation for materials in which both elastic and plastic strains are large requires special analyses.[11,18]

Two separate cases of work hardening, characterized by different work-hardening rates $\eta = d\sigma/d\epsilon$, were considered. In one, elastic perfectly-plastic behavior was assumed ($\eta = 0$), and in the other, a moderate rate of work hardening was used which increases the flow stress by a factor of 2 at 10% plastic strain ($\eta = 10\ \sigma_y$). The yield strengths and work hardening rates examined in the study approximate the behavior a wide range of metals and ceramics.

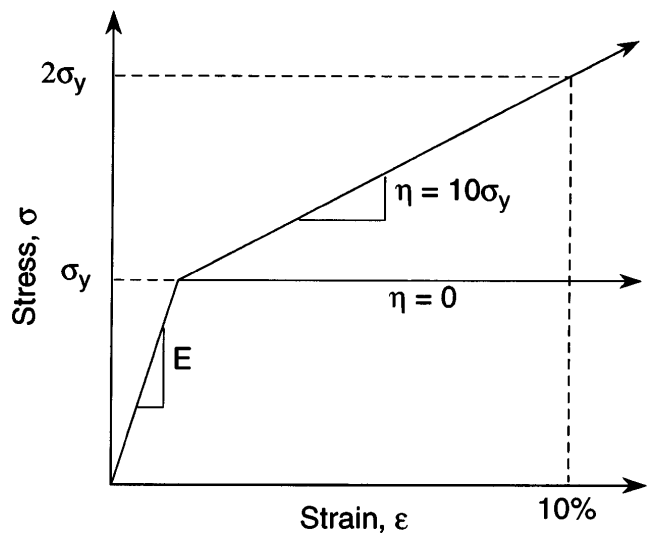

FIG. 2. A schematic representation of the constitutive behavior used in the finite element modeling.

The output of the finite element simulations included indentation load-displacement curves during one cycle of loading and unloading, the shapes of contact impressions, and the geometries of plastic zones. To implement the Oliver–Pharr data analysis procedures, the unloading curves were fit according to Eq. (1), and the curve-fitting parameters were used in Eq. (2) to determine the unloading stiffnesses. Noting that (1) the indenter used in the study was perfectly rigid ($E_i = \infty$), (2) the best empirical value for ϵ for a sharp indenter is 0.75,[3] and (3) the shape function for a perfect cone is given by $A = \pi d^2 \tan^2 \phi$ where $\phi = 70.3°$, Eqs. (3)–(6) yield the following simplified expressions for the contact area, hardness, and elastic modulus:

$$A = \pi\left(h_{\max} - 0.75\,\frac{P_{\max}}{S}\right)^2 \tan^2 70.3° \tag{7}$$

$$H = \frac{P_{\max}}{A} \tag{8}$$

$$E = (1 - \nu^2)\,\frac{\sqrt{\pi}}{2}\,\frac{S}{\sqrt{A}}\,. \tag{9}$$

These equations were used to compute the parameters of interest from the finite element load-displacement results. Note that the finite element simulations generate two separate measures of the contact area: one inferred from the load-displacement data through Eq. (7) and the other a more direct measure obtained by examination of

the contact profile in the finite element mesh. Throughout this work, each of these will be used in the computation of H and E, with the former referred to as $A_{O/P}$ to denote that it was derived from the load-displacement data using the Oliver–Pharr method, and the latter, which represents the true area of contact, referred to as A_{true}. Unless otherwise noted, the contact areas are those obtained with the indenter fully loaded into the specimen. This distinction is important because the radial position of last point of contact at the indenter/specimen interface changes slightly during unloading due to elastic recovery. The contact area at full load is preferred to facilitate comparison to the area derived using the Oliver–Pharr procedures, which is the area at full load.

III. RESULTS AND DISCUSSION

A. Load-displacement curves

Figure 3 shows examples of typical indentation load-displacement curves generated in the finite element simulations. The two curves represent important extremes in material behavior; while both sets of data were generated using $E = 70$ GPa, $\nu = 0.25$, and $\eta = 0$ (i.e., no work hardening), the materials differ substantially in their yield stresses. The relatively high yield stress for the material in Fig. 3(a), $\sigma_y = 2662$ MPa, results in a material of relatively high hardness. The hardness computed from Eq. (8) using the true area of contact is $H = 5.82$ GPa, which in conjunction with the 70 GPa modulus makes this material mechanically similar to soda-lime-silicate glass.[3] On the other hand, the relatively low yield stress of 228.5 MPa for the material in Fig. 3(b) produces a low hardness, $H = 0.60$ GPa, and the mechanical properties of this material are more like those of aluminum.[3] When considered in terms of their modulus-to-hardness ratios, E/H, or their effective modulus-to-yield strength ratios, E_{eff}/σ_y, these two materials represent extremes in behavior. For the glass-like material [Fig. 3(a)], $E/H = 12.0$ and $E_{eff}/\sigma_y = 28.1$, whereas for the aluminum-like material [Fig. 3(b)], $E/H = 117.5$ and $E_{eff}/\sigma_y = 327$. A recent compilation of experimental data shows that E/H is rarely less than 10 or more than 150 for a wide variety of metals, ceramics, and polymers.[19] Thus, the glass-like material is on the low end of the E/H spectrum while the aluminum-like material is near the high end.

The differences in the magnitudes of the yield stresses and the modulus-to-yield strength ratios of the two materials manifest themselves in the two important ways in the indentation load-displacement behavior of Fig. 3. First, the load needed to drive the indenter to the same depth is much greater for the glass, as would be expected from its much greater yield strength. Second, the portion of the indenter displacement which is elastically recovered during unloading is also much greater for the glass. As discussed in detail elsewhere,[16,17] the amount of elastic recovery can be conveniently characterized by the ratio of the final indentation depth to the maximum indentation depth, h_f/h_{max}. This parameter, which is independent of indentation depth because of the self-similar geometry of the indenter, is easily measurable from experimental data. The natural limits for the parameter are $0 \leqslant h_f/h_{max} \leqslant 1$. The lower limit corresponds to fully elastic deformation and thus complete recovery of the indentation displacements during unloading. The upper limit is characteristic of a rigid-plastic material, for which there is no elastic recovery. The values of h_f/h_{max} for the materials in Fig. 3 are 0.687 for the glass and 0.951 for the aluminum.

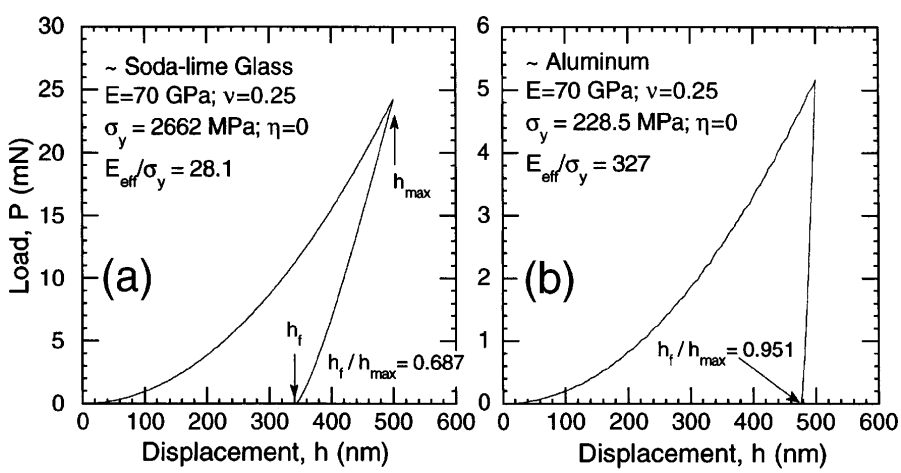

FIG. 3. Simulated indentation load-displacement curves for: (a) a material similar to soda-lime glass with $E_{eff}/\sigma_y = 28.1$; (b) a material similar to aluminum with $E_{eff}/\sigma_y = 327$.

From a purely mechanical standpoint, the fundamental material parameters controlling elastic/plastic deformation during indentation are the elastic constants, E and ν, the yield stress, σ_y, and the work-hardening rate, η. Thus, perhaps the most natural way to present the finite element results is in the way they vary with E, ν, σ_y, and η. However, during the course of this investigation, it was found that a simple and useful correlation exists between the fundamental material parameters and the experimentally measurable $h_f/h_{\max}$. The correlation is shown in Fig. 4, which plots the dependence of $h_f/h_{\max}$ on $E_{\text{eff}}/\sigma_{10\%}$, the ratio of the effective elastic modulus to the flow stress at 10% strain, $\sigma_{10\%}$. When plotted this way, finite element simulation data for a wide variety of materials with different E/σ_y values converge to a single master curve, with Poisson effects producing only minor deviations. The use of flow stress at 10% strain as a normalizing parameter was inspired by Tabor's observations that the effects of work hardening on the Vickers hardness of metals can often be accounted for by replacing the yield stress with the flow stress at a characteristic strain, usually in the range 8–20%.[20] In the current study, the best correlation was achieved using the flow stress at 10% strain. The importance of the correlation is that it uniquely relates the fundamental material deformation parameters E, ν, σ_y, and η to a parameter which can be simply and accurately measured in experiment. Since E, ν, σ_y, and η are not known *a priori* in a nanoindentation experiment, the variation of parameters derived in the finite element simulations with $h_f/h_{\max}$ provides a useful way to link the finite element results to experimental behavior. As a consequence, most of the important relationships derived in this work are presented as a function of $h_f/h_{\max}$. Dependencies on the more fundamental material parameters can be achieved through the correlation given in Fig. 4.

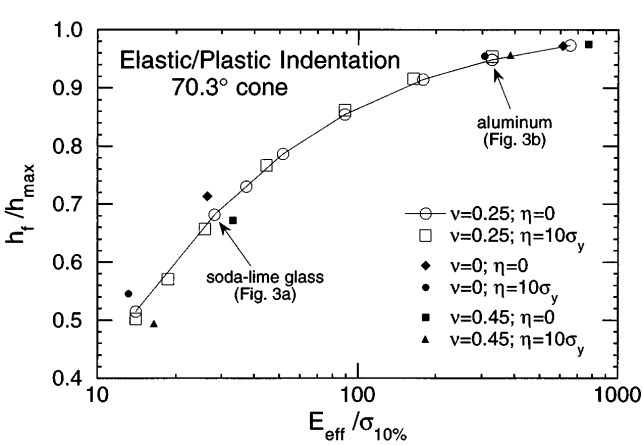

FIG. 4. The dependence of $h_f/h_{\max}$ on $E_{\text{eff}}/\sigma_{10\%}$.

B. Surface profiles and contact areas

Figure 5 shows geometric cross sections of fully loaded indentations to illustrate important differences in the pileup and sink-in behavior of materials having $\nu = 0.25$. The figure shows that whether the material piles up or sinks in depends on both $h_f/h_{\max}$ (or, alternatively, E, ν, σ_y, and η) and the work-hardening characteristics of the material. Of the materials modeled in this study, pileup is most significant in those that do not work harden and for which $h_f/h_{\max}$ is close to 1. On the other hand, sink-in occurs, irrespective of the work-hardening characteristics, when $h_f/h_{\max} < 0.7$. The moderate amount of work hardening examined in this study promotes sink-in in preference to pileup at all $h_f/h_{\max}$. Similar observations of the effects of work hardening on pileup and sink-in have been made in three-dimensional finite element studies of indentation with Vickers and Berkovich indenters.[14,15,18] Figure 6 is included to show that varying Poisson's ratio in the range

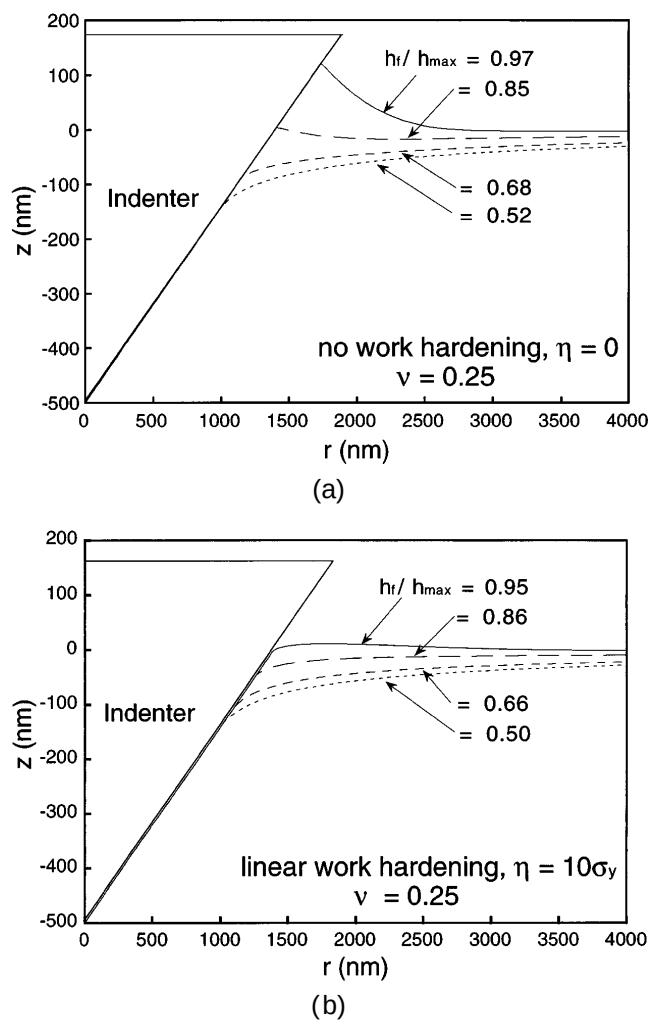

FIG. 5. Indentation contact profiles for: (a) non-work hardening materials ($\eta = 0$); (b) work-hardening materials ($\eta = 10\ \sigma_y$).

$0 \leqslant \nu \leqslant 0.45$ has only minor influences on the contact profiles. The profiles shown in Fig. 6 are for non-work hardening materials; when the material work hardens, the differences are even smaller.

The contact profiles in Fig. 5 take on special significance when considered in the ways they affect the projected contact areas, as shown in Fig. 7. This figure includes both the contact areas determined directly from the finite element mesh, A_{true}, and the contact areas derived from the load-displacement data using the Oliver–Pharr analysis procedure, $A_{\text{O/P}}$ [computed from Eq. (7)]. To generalize the results, each area has been normalized with respect to the area given by the indenter shape function, A_{sf}, evaluated at the maximum indentation depth, $h_{\max}$. Since A_{sf} is the area that would be observed if no pileup or sink-in occurred at all, values of $A_{\text{true}}/A_{\text{sf}}$ greater than 1 indicate a tendency for the material to pile up while values less than 1 suggest that the material sinks in.

Focusing first in Fig. 7 on the true contact areas, A_{true}, a number of points are noteworthy. First, at small values of $h_f/h_{\max}$, the limit of purely elastic contact is approached, and the data appear to be in reasonable agreement with limiting value $A_{\text{true}}/A_{\text{sf}} = 0.405$ predicted by Sneddon's analysis for the indentation of an elastic half-space by a rigid cone.[6] For large values of $h_f/h_{\max}$, A_{true} depends strongly on the work-hardening characteristics of the material. With no work hardening, there is a large amount of pileup, as evidenced by increases in $A_{\text{true}}/A_{\text{sf}}$ with $h_f/h_{\max}$ to values greater than 1.5. This means that more than 50% of the contact area in non-work hardening materials can result from pileup. Lockett's slip line field analysis for deformation of a rigid/plastic material by a conical indenter shows the limiting value of $A_{\text{true}}/A_{\text{sf}}$ to be 1.70,[21] which is consistent with the trends in the finite element data. On the other hand, for work-hardening materials, the tendency for material to pileup is not nearly as strong. In fact, close examination of Fig. 7 shows that all of the $A_{\text{true}}/A_{\text{sf}}$ values for work-hardening materials are less than 1.0. Another noteworthy point is that the deviation in contact areas for the work-hardening and non-work hardening materials occurs at $h_f/h_{\max} \approx 0.7$; below this value, the work-hardening characteristics do not appreciably influence the observed contact areas.

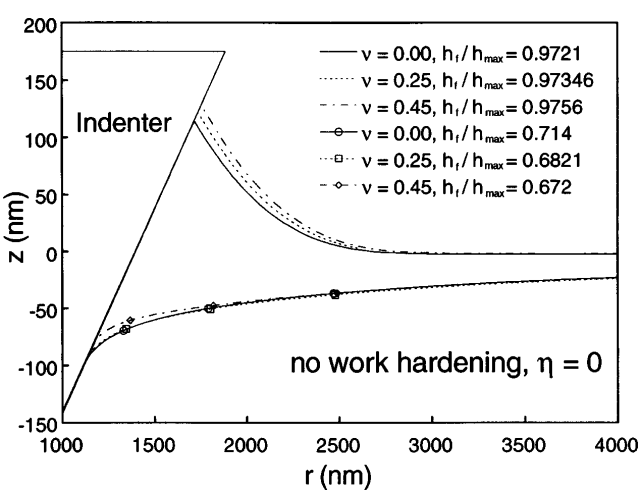

FIG. 6. Indentation contact profiles for non-work hardening materials showing the influences of Poisson's ratio on the contact geometry.

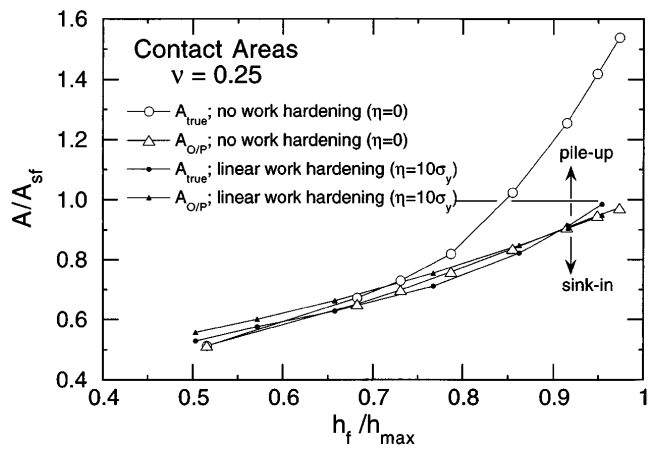

FIG. 7. The dependence of the contact areas derived from the finite element simulations on $h_f/h_{\max}$. The contact areas, A, are normalized with respect to A_{sf}, the area given by the indenter shape function evaluated at the contact depth.

A comparison of the true contact areas in Fig. 7 with those derived from the Oliver–Pharr analysis procedure can now be used to gain an appreciation of the conditions under which pileup leads to significant errors in contact areas derived by the Oliver–Pharr method. It should be recalled that since the Oliver–Pharr method is based on a strictly elastic analysis which can account for sink-in only, the method may fail to adequately predict contact areas for materials in which pileup occurs. The results of Fig. 7 demonstrate that this is indeed the case and help to identify those materials in which pileup is an important factor. Specifically, a significant deviation in A_{true} and $A_{\text{O/P}}$ occurs for non-work hardening materials when $h_f/h_{\max} > 0.7$. For these materials, the Oliver–Pharr method underestimates the contact area by as much as 60%. On the other hand, when $h_f/h_{\max} < 0.7$, the Oliver–Pharr method provides a reasonable estimate of the contact area, irrespective of the work-hardening behavior. Note that from an experimental point of view, it is not possible to predict if a material work hardens based solely on the indentation load-displacement data. Therefore, in measuring mechanical properties by load and depth sensing methods, care must be exercised when $h_f/h_{\max} > 0.7$, since use of the Oliver–Pharr method can lead to significant errors in the contact area.

C. Hardness

Since hardness and contact area are related to each other in a simple reciprocal manner [Eq. (8)], the errors in contact area caused by not accounting for pileup manifest themselves in similar errors in the hardness. Figure 8 shows the dependence of $H/\sigma_{10\%}$, the hardness normalized with respect to the flow stress at 10% strain, on $h_f/h_{\max}$. Included in the plot are hardnesses computed using the true area of contact, H_{true}, as well as hardnesses computed using the area derived from the Oliver–Pharr procedure, $H_{\text{O/P}}$. As would be expected based on the contact area observations, the Oliver–Pharr method predicts the hardness reasonably well for all materials except those that do not work harden and for which $h_f/h_{\max} > 0.7$. For these materials, the Oliver–Pharr method overestimates the hardness by as much as 60%.

The finite element results in Fig. 8 can also be used to expand upon the well-known relation between hardness and flow stress proposed by Tabor.[20] Using the results of slip line field analyses for rigid/plastic deformation, Tabor suggested that the Vickers hardness of a metal is approximately 2.9–3.0 times its flow stress at 8–10% strain; that is, $H \cong C\sigma_{8-10\%}$ where $C = 2.9$–3.0. Since rigid/plastic behavior corresponds to $h_f/h_{\max} = 1$, how well the Tabor relation compares to the finite element simulation results can be established by examining the values of $H/\sigma_{10\%}$ at large $h_f/h_{\max}$. Inspection of Fig. 8 shows that for the non-work hardening materials, $H_{\text{true}}/\sigma_{10\%}$ plateaus at a value of about 2.6, whereas for the work-hardening materials, $H_{\text{true}}/\sigma_{10\%}$ rises continuously to about 3.0. Thus, while the Tabor relation appears to work reasonably well, the finite element results suggest that the constant C for non-work hardening materials is closer to 2.6 than it is to 3.0. The results in Fig. 8 also show how the constant C is close to 3.0 only for a limited range of materials, specifically those for which $h_f/h_{\max}$ is near 1. According to Fig. 4, these materials are those with large values of $E_{\text{eff}}/\sigma_{10\%}$, which occurs only in materials with a relatively high modulus and low hardness, e.g., soft metals. For hard metals and most ceramics, glasses, and polymers, $E_{\text{eff}}/\sigma_{10\%}$ is generally much smaller, and a smaller value of C applies. For a specific material, the results of Fig. 8 can be used to estimate C from a knowledge of $h_f/h_{\max}$ obtained in a load and depth sensing indentation experiment, or alternatively, by knowing E, ν, σ_y, and η, and deducing the associated value of $h_f/h_{\max}$ through the correlation in Fig. 4.

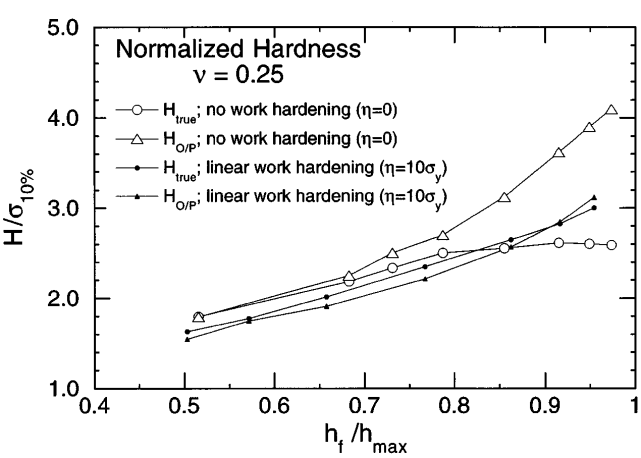

FIG. 8. The dependence of $H/\sigma_{10\%}$ on $h_f/h_{\max}$ for non-work hardening materials ($\eta = 0$) and work-hardening materials ($\eta = 10\ \sigma_y$).

D. Elastic modulus

As in the case of hardness, pileup can also significantly affect the measurement of elastic modulus by the Oliver–Pharr method. To illustrate this, Fig. 9 shows the dependence of E_{eff} on $h_f/h_{\max}$, where E_{eff} has been calculated from Eq. (9) using the two different measures of the contact area, $A_{\text{O/P}}$ and A_{true}. The effective moduli shown in the plot are normalized with respect to the modulus used as input into the finite element code. As one would expect based on the contact area observations in Fig. 7, for non-work hardening materials with $h_f/h_{\max} > 0.7$, the effective modulus computed using $A_{\text{O/P}}$ is significantly overestimated; the overestimation is as great as ~50% when $h_f/h_{\max}$ is close to 1 (i.e., pileup is very large). Curiously, however, the figure also shows that even when pileup is not important, i.e., when $h_f/h_{\max} < 0.7$, the effective modulus determined by the Oliver–Pharr method is still 5–10% greater than that used as input into the finite element code. Moreover, the overestimation occurs even when the true contact area is used for the modulus computations. The origin of this behavior is addressed separately,[22] where it is shown that a correction to Eq. (9) is needed to properly apply Sneddon's elastic solution to data obtained with a conical indenter. The magnitude of the correction depends on Poisson's ratio of the specimen, ν, and the cone angle of the indenter, ϕ. For $\nu = 0.25$ and $\phi = 70.3°$, the correction reduces the computed effective modulus by about 7%, which is close to what is needed to correct the moduli measured in the current work to their expected values. Thus, when $h_f/h_{\max} < 0.7$, there is an explanation for the overestimation of moduli deduced from Eq. (9).

The same is not true, however, when $h_f/h_{\max} > 0.7$. In this range, use of the true contact area to compute E_{eff} by means of Eq. (9) results in an effective modulus which is overestimated by as much as 16%. This value is too large to be accounted for by the 7% correction. This means that when $h_f/h_{\max} > 0.7$, plastic deformation during indentation affects the load-displacement behavior in such a way that an accurate

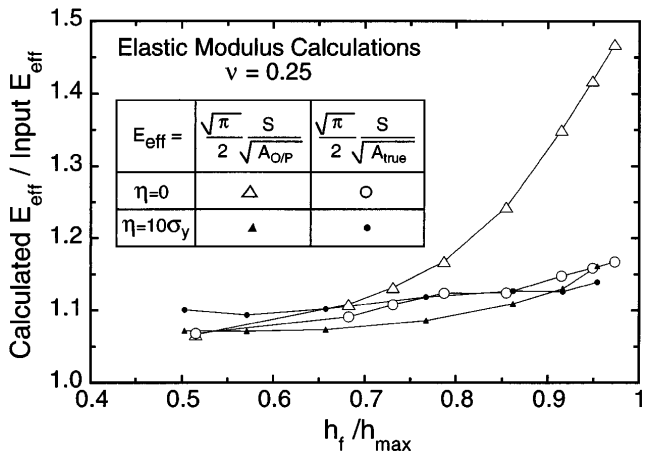

FIG. 9. The dependence of the effective elastic moduli derived from the finite element results on $h_f/h_{\max}$. The calculated effective moduli are normalized with respect to the effective elastic modulus input into the finite element code.

analysis can no longer be achieved by means of elastic solutions only. Thus, some error is to be expected in the measured modulus. The finite element results in Fig. 9 can be used to provide a first-order correction for this problem.

E. Plastic zones

Important physical insights into the finite element results can be gained by examining the behavior of the plastic zones at the indentation contacts. Figure 10 shows the plastic zones for materials with four different values of E_{eff}/σ_y ($\nu = 0.25$ in all cases). The progression from left to right across the figure corresponds to decreasing E_{eff}/σ_y, which was accomplished in the finite element simulations by increasing the yield stress while holding the modulus constant. Note that the x and y axes are scaled in the same way in order to provide an undistorted picture of the proportions and shapes of the zones. The two arrows pointing to the surface in each figure mark the contact perimeters for the cases $\eta = 0$ (arrow on the right) and $\eta = 10\ \sigma_y$ (arrow on the left). The values of $h_f/h_{\max}$ shown in the figure are for materials with no work hardening ($\eta = 0$).

The plastic zones for non-work hardening materials ($\eta = 0$) are shown as solid lines in Fig. 10. Starting at the left with the largest $E_{\text{eff}}/\sigma_y = 326$, corresponding to the smallest yield stress and the largest $h_f/h_{\max} = 0.95$, it is seen that the plastic zone extends well beyond the circle of contact. As discussed previously, it is in materials such as this that extensive pileup leads to significant errors in the measurement of A, H, and E by the Oliver–Pharr method. As E_{eff}/σ_y decreases, corresponding to increases in the yield stress and decreases in $h_f/h_{\max}$, the size of the plastic zone decreases until, at some point, the plastic zone boundary in the surface coincides with the contact perimeter. Interestingly, the value of $h_f/h_{\max}$ at which this occurs is between 0.68 and 0.73, that is, at the transition from pileup to sink-in behavior (see Figs. 5 and 7). For very small values of E_{eff}/σ_y, e.g., $E_{\text{eff}}/\sigma_y = 14.3$ [Fig. 10(d)], the plastic zone boundary lies inside the contact perimeter. It thus appears, at least for non-work hardening materials, that whether a material piles up or sinks in during indentation has an interesting correlation to the size of the plastic zone. Specifically, when the plastic zone extends beyond the circle of contact, pileup is large, but when the plastic zone lies inside the contact perimeter, deformation outside the contact is purely elastic and sink-in occurs.

The behavior for work-hardening materials is different. As noted by Johnson,[23] a large capacity for work hardening drives the plastic zone into the material to greater depths and decreases the amount of pileup adjacent to the indenter. This is corroborated in Fig. 10, where the broken lines show the plastic zones for work-hardening materials ($\eta = 10\ \sigma_y$) with the same E_{eff}/σ_y ratios as the non-work hardening materials. The plastic zones for the work-hardening materials are clearly driven in to greater depths, but an equally important effect is that work hardening tends to reduce the radius of the plastic zone in the surface. This is particularly apparent in Fig. 10(b). Furthermore, as in the case of non-work hardening materials, when the radius of the plastic zone approaches the radius of contact, pileup is minimal and the vertical displacement of the edge of the contact is determined by elastic deformation outside the plastic zone. Of the materials examined in Fig. 10, only for the conditions in Fig. 10(a) is there any evidence of plastic flow outside the contact perimeter, and even in this case, the amount pileup is small. It is because of this that the Oliver–Pharr analysis procedure provides a good estimate of the contact area over a wider range of $h_f/h_{\max}$ for work-hardening materials.

F. Power law exponents

To conclude, one last observation is presented which, while not directly related to the subject of pileup, offers important insights into the nature of unloading curves obtained in load and depth sensing indentation experiments. In particular, it is well documented that the unloading curves of a wide variety of metals and ceramics tested with geometrically similar indenters like the Berkovich are well described by the power-law relation of Eq. (1) with power law exponents, m, in the range 1.2 to 1.5.[3] Figure 11 shows how the exponents determined from power law fits of the unloading curves generated in the finite element simulations vary with $h_f/h_{\max}$. For $h_f/h_{\max}$ in the range 0.5 to 1, which covers

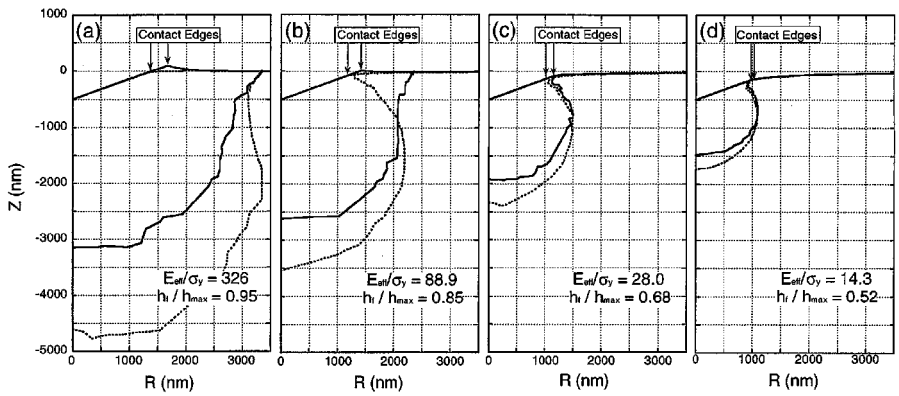

FIG. 10. Plastic zones developed during indentation for various values of $E_{\mathrm{eff}}/\sigma_y$. Non-work hardening materials ($\eta = 0$) are represented by solid lines and work-hardening materials ($\eta = 10\ \sigma_y$) by broken lines.

the experimental behavior of most metals and ceramics, the exponents predicted by the finite element simulations are quite similar to those observed in experiment ($1.2 < m < 1.5$). The finite element results thus suggest that it is not necessary to appeal to indenter tip rounding, as has been done in the past,[3] to explain why power law exponents are less than 2,[3] the theoretical limit for indentation of an elastic half space by a cone.[6] Rather, the lower exponents are a consequence of the complex elastic-plastic deformation processes occurring during indentation and are expected even for a sharp, geometrically similar indenter such as a cone. Recent three-dimensional finite element studies of Vickers indentation also bear this out,[18] although the unloading curves in these studies were not found to be well represented by power laws over the entire range of displacement, in contrast to the current finite element results and actual experimental behavior.[3] The results in Fig. 11 also suggest that some variability is expected in the power law exponent depending on the elastic and plastic properties of the material.

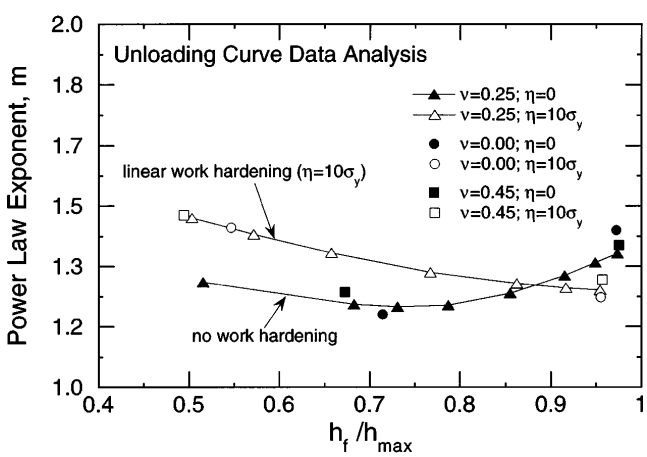

FIG. 11. The dependence of the power law exponent, m, on $h_f/h_{\max}$.

IV. CONCLUSIONS

The results of a finite element study of conical indentation of elastic-plastic materials have shown that pileup can have important influences on the measurement of contact area, hardness, and elastic modulus by load and depth-sensing indentation methods. The parameter $h_f/h_{\max}$, which can be measured experimentally and correlates with the material parameters E, ν, σ_y, and η which control indentation deformation, can be used as an indication of when pileup is an important factor. Pileup is significant only when $h_f/h_{\max} > 0.7$ *and* the material does not appreciably work harden. For such materials, failure to account for the pileup can lead to an underestimation of the contact area deduced from indentation load-displacement data by as much as 60%. This, in turn, results in an overestimation of the hardness and elastic modulus. When $h_f/h_{\max} < 0.7$, or in all materials that moderately work harden, pileup is not a significant factor, and the Oliver–Pharr data analysis procedure can be expected to give reasonable results.

The finite element results also provide further insights into the relation between hardness and flow stress proposed by Tabor, $H \cong C\sigma_{8\text{-}10\%}$.[20] For materials with large $E_{\mathrm{eff}}/\sigma_{10\%}$ ratios, such as soft metals, the Tabor relation works reasonably well, although the finite element results suggest that the constant C for materials that do not work harden may be closer to 2.6 than it is to 2.9–3.0 as suggested by Tabor. On the other hand, for materials with small $E_{\mathrm{eff}}/\sigma_{10\%}$ ratios, such as hard metals and most ceramics, glasses, and polymers, the finite element simulations show that a smaller value of C applies, the value of which can be estimated from a measurement of $h_f/h_{\max}$ in a load and depth-sensing indentation experiment.

Finally, the finite element results show that the unloading curves of materials tested with a conical indenter should be well described by a power-law relationship with power law exponents, m, in the range 1.2 to

1.5, in accordance with experimental studies of a wide variety of metals and ceramics tested with geometrically similar indenters like the Berkovich. The fact that power law exponents are less than 2, the value expected for conical indentation of an elastic half-space, is a natural consequence of the complex elastic/plastic deformation occurring at the indentation. It is thus not necessary to invoke indenter tip-rounding effects to explain the origin of exponents less than 2, as has been proposed in previous work.[3]

ACKNOWLEDGMENTS

This research was sponsored by the Division of Materials Science, United States Department of Energy, under contract DE-AC05-96OR22464 with Lockheed Martin Energy Research Corp., and through the SHaRE program under contract DE-AC05-76OR00033 with the Oak Ridge Associated Universities. The authors wish to thank Dr. Warren C. Oliver for valuable input. One of the authors (GMP) is grateful for sabbatical support provided by the Oak Ridge National Laboratory.

REFERENCES

1. J.L. Loubet, J.M. Georges, O. Marchesini, and G. Meille, J. Tribology **106**, 43 (1984).
2. M.F. Doerner and W.D. Nix, J. Mater. Res. **1**, 601 (1986).
3. W.C. Oliver and G.M. Pharr, J. Mater. Res. **7**, 1564 (1992).
4. J.B. Pethica, R. Hutchings, and W.C. Oliver, Philos. Mag. A **48**, 593 (1983).
5. G.M. Pharr and W.C. Oliver, MRS Bull. **17**, 28 (1992).
6. I.N. Sneddon, Int. J. Engng. Sci. **3**, 47 (1965).
7. T.Y. Tsui, W.C. Oliver, and G.M. Pharr, J. Mater. Res. **11**, 752 (1996).
8. A. Bolshakov, W.C. Oliver, and G.M. Pharr, J. Mater. Res. **11**, 760 (1996).
9. A.K. Bhattacharya and W.D. Nix, Int. J. Solids Struct. **24**, 881 (1988).
10. A.K. Bhattacharya and W.D. Nix, Int. J. Solids Struct. **24**, 1287 (1988).
11. T.A. Laursen and J.C. Simo, J. Mater. Res. **7**, 618 (1992).
12. A. Bolshakov, W.C. Oliver, and G.M. Pharr, in *Thin Films: Stresses and Mechanical Properties V,* edited by S.P. Baker, C.A. Ross, P.H. Townsend, C.A. Volkert, and P. Børgesen (Mater. Res. Soc. Symp. Proc. **356**, Pittsburgh, PA, 1995), p. 675.
13. D.T. Madsen, R.J. Giovinazzo, J.E. Ritter, and T.J. Lardner, in *Thin Films: Stresses and Mechanical Properties III,* edited by W.D. Nix, J.C. Bravman, E. Arzt, and L.B. Freund (Mater. Res. Soc. Symp. Proc. **239**, Pittsburgh, PA, 1992), p. 431.
14. A.E. Giannakopoulos, P-L. Larsson, and R. Vestergard, Int. J. Solids Struct. **31**, 2679 (1994).
15. P-L. Larsson, A.E. Giannakopoulos, E. Soderlund, D.J. Rowcliffe, and R. Vestergaard, Int. J. Solids Struct. **33**, 221 (1996).
16. A. Bolshakov, W.C. Oliver, and G.M. Pharr, in *Thin Films: Stresses and Mechanical Properties VI,* edited by W.W. Gerberich, H. Gao, J-E. Sundgren, and S.P. Baker (Mater. Res. Soc. Symp. Proc. **436**, Pittsburgh, PA, 1997), p. 141.
17. A. Bolshakov, Ph.D. Dissertation, Rice University, May 1996.
18. A.E. Giannakopoulos and P-L. Larsson, Mech. Mater. **25**, 1 (1997).
19. A. Bolshakov and G.M. Pharr, unpublished.
20. D. Tabor, *The Hardness of Metals* (Oxford University Press, London, 1951).
21. F.J. Lockett, J. Mech. Phys. Solids **11**, 345 (1963).
22. A Bolshakov and G.M. Pharr, in *Thin Films: Stresses and Mechanical Properties VI,* edited by W.W. Gerberich, H. Gao, J-E. Sundgren, and S.P. Baker (Mater. Res. Soc. Symp. Proc. **436**, Pittsburgh, PA, 1997), p. 189.
23. K.L. Johnson, *Contact Mechanics* (Cambridge University Press, Cambridge, 1985).